Overhanging ferroelectric nanodot arrays created by high surface energy seeds

Jiyoon Kim[a], Kwang-Won Park[b], Jongin Hong[b,*], Kwangsoo No[a,*]

[a] Department of Materials Science and Engineering, KAIST, Daejeon 305-701, Republic of Korea
[b] Department of Chemistry, Chung-Ang University, Seoul 156-756, Republic of Korea

ARTICLE INFO

ABSTRACT

We demonstrated a facile route for the fabrication of overhanging PbTiO$_3$ (PTO) nanodot arrays on platinized silicon substrates using PbO vapor phase reaction sputtering on micellar monolayer films of polystyrene-block-poly(ethylene oxide) (PS-*b*-PEO) loaded with TiO$_2$ sol–gel precursor. We also investigated that the high surface energy of TiO$_2$ contributes to the formation of overhanging ferroelectric PTO nanodot arrays by means of high-resolution transmission electron microscopy. Additionally, the crystallographic orientation of the nanoseeds had a significant influence on the ferroelectric switching properties of the PTO nanodots, which were determined by piezoresponse force microscopy (PFM).

1. Introduction

It is an undeniable fact that the ferroelectric materials have been extensively investigated due to their unique features, such as spontaneous electric polarization, high dielectric permittivity, pyroelectricity and piezoelectricity, for practical applications [1,2]. For example, the spontaneous polarization is crucial for non-volatile memory functions. Its temperature dependence is utilized for ultrasensitive infrared detectors. Piezoelectricity is applied to high performance actuators and energy harvesters [3,4]. In particular, switchable polarization is a basic requirement in the application of information storage devices, where the desired information (one bit) can be deposited by assigning a polarization direction under suitable electric fields greater than the coercive value of E_c [5]. What interests us is that zero-dimensional (0D) nanostructures differ from three-dimensional microstructures or bulk structures in terms of their electric properties. To date, various methods have been introduced to obtain a high level of memory density in two-dimensional (2D) ferroelectric thin films; however, the collapse or crosstalk of ferroelectric domains written in the thin films is treated as a serious problem when aiming to achieve memory density greater than 1 Tb/in^2 [2,6,7]. Recently, discrete 0D nanostructures have been proposed to minimize size effects on ferroelectric properties and to overcome the instability of stored information in the continuous film [8]. The physically separate geometry would also act as an intrinsic barrier to avoid overlapping between electric fields when reading and writing data and unexpected domain wall propagation towards neighbors.

Ferroelectric properties typically vanish below a critical size of 10 nm and this is known as the finite size effect [9]. It should be noted that the discrete 0D nanostructure is very attractive for enhancing the ferroelectric properties since it reduces the clamping effect from a substrate [10]. Accordingly, it is of significant importance to create a structure with less contact area between ferroelectric materials and the underlying substrate. Since the mid-1990s, classical top-down approaches, such as focused ion beam (FIB) milling and electron beam direct writing (EBDW), have been employed to pattern surface into an array of individual ferroelectric materials [11,12]. However, for they are time-consuming and low-throughput processes, several alternative bottom-up approaches such as dip-pen lithography and the use of block copolymers as nanoscale templates have been introduced to explore stable ferroelectric nanostructures smaller than 100 nm [13,14]. Despite such recent advances, there still lies a necessity to employ a post-annealing treatment at an elevated temperature in order to crystallize ferroelectric materials; extra caution is to be taken when doing this, since this could beget undesirable alterations in shape or in volume of the ferroelectric nanostructures. We anticipate that the ideal shape to minimize the clamping effect would be a sphere rather than an islet. However, both top-down and bottom-up approaches would not be feasible for preparing spherical ferroelectric nanodots. Herein, we describe the benefit of an

* Corresponding authors.
E-mail addresses: hongj@cau.ac.kr (J. Hong), ksno@kaist.ac.kr (K. No).

indirect deposition of ferroelectric materials to create overhanging PbTiO$_3$ (PTO) nanodot arrays by combining PbO gas phase reaction with nanoscale TiO$_2$ seeds. We infer that the high surface energy of the TiO$_2$ would contribute to the formation of spherical nanodot arrays.

2. Experimental

Polycrystalline PTO and nanodot arrays (40 nm in height and 60 nm in diameter) were prepared on platinized silicon substrates by the reaction between TiO$_2$ in a solid phase and PbO in a gas phase. Spherical TiO$_2$ nanoseeds were too prepared by self-ordered micellar monolayer films. In order to obtain precursor-loaded inverse micelles, a polystyrene-*block*-poly(ethylene oxide) (PS-*b*-PEO) copolymer solution was arranged by dissolving PS-b-PEO (40 mg) in toluene (2 mL) and a sol–gel precursor was generated by mixing HCl (10 mg) and titanium tetra-isopropoxide (TTIP, 72 mg) in isopropyl alcohol (IPA, 1 mL). 1 mL of the copolymer solution was then combined with 0.3 mL of the sol–gel precursor solution. The inverse micelles were spin-coated on platinized silicon substrates using an ACE-200 spin coater (Dongah Tech., Korea) under ambient conditions (2500 rpm or rotation speed and 1250 rpm/s of acceleration speed). The polymer templates were eliminated by oxygen plasma etching and then PbO was reacted with the TiO$_2$ seeds by RF reactive magnetron sputtering at 600 °C in an O$_2$ atmosphere.

The crystalline orientation of the TiO$_2$ and PTO nanodot arrays was determined by X-ray diffraction (XRD, D/MAX-RC, Rigaku Co.) with a 2θ scan at 40 kV and 100 mA. Conventional transmission electron microscopy (TEM) and high-resolution TEM analysis were then performed by a JEOL FB-2100F microscope at 200 kV, followed by the preparation of the cross-sectional TEM samples by focused ion beam (FIB) milling. Pt was deposited on the upper surface of epoxy-covered nanodots to keep the underlying sample intact from the destructive sputtering of the ion beam. The local piezoresponse hysteresis loop was obtained at a fixed position in terms of photodiode voltage output as a function of dc bias voltage, which was applied to the bottom electrode (sequence 0 V → −5 V → 0 V → +5 V → 0) and was superimposed onto the ac modulation voltage applied to the tip [14,15]. We randomly selected 10 PTO nanodots for measuring the loops and averaged them for evaluating the local piezoresponse.

3. Results and discussion

The TiO$_2$ nanodots were successfully transformed into the PTO nanodots without using costly lithographic tools. It is notable that TiO$_2$ nanodot arrays would provide reaction sites to capture PbO molecules with ease and this thereby allowed a fall in the formation temperature of a ferroelectric phase. Moreover, we thought that the TiO$_2$ seeds would play a key role for determining the final shape of the ferroelectric nanodots since the surface energy of TiO$_2$ (i.e. 2.6 J/m^2 for (1 0 1) and 3.7 mJ/m^2 for (1 0 0)) is greater than that of underlying Pt (i.e. 2.2–2.3 J/m^2) [16,17]. Fig. 1 illustrates classical wetting and contact angles in a vapor–liquid–solid system at equilibrium. The shape of the liquid on the solid substrate conforms to the minimum interface energy. The liquid forms a ball to reduce the interface between solid and liquid, when the interface energy between them is high (Fig. 1a). With an incompressible solid, the balance of forces which determines the contact angle can be expressed as $Cos\theta = \frac{(\gamma_{SV} - \gamma_{SL})}{\gamma_{LV}}$ where γ, θ, S, L and V denote interface energy, contact angle, solid, liquid and vapor, respectively. When two distinct materials meet, they compete with each other to reduce high-energy surface. In particular, wetting of nanoscale seeds on an underlying substrate at an elevated temperature relies on both surface energies of seeds and underlying materials, and the wetting is driven to minimize the total interfacial energy in the system. Fig. 1d and e indicates schematics of nano-islands and overhanging nanodots where contact angles are small (i.e. large contact area) and large (i.e. small contact area), respectively. The nano-island appears when the surface energy is less than that of the underlying material, whilst the overhaning nanodot is preferential in the opposite situation. Regardless of various preparation methods, islet nanostructures of PbTiO$_3$ have been reported in the literature [18–20]. If we create spherical nanostructures holding a contact angle larger than 90°, the surface energy of the ferroelectric material should be greater than that of the underlying substrate. The calculated surface energy density (SED) of PbTiO$_3$ is 1.0–2.0 J/m^2 and this value are comparable with that of common conductive substrates (i.e. 1.4–3.0 J/m^2 of SrTiO$_3$ and 2.2–2.3 J/m^2 of Pt) [21,22]. Thus, we anticipate that island-like nanostructures would be preferred. Interestingly, this coincides with the resultant shapes found in the literature.

Fig. 2a shows a scanning electron microscopy (SEM) image of highly cross-packed and spherical PTO nanodot arrays prepared by the selective growth of ferroelectric oxides on nanoscale TiO$_2$ seeds. Their cross-sectional TEM images are also displayed in Fig. 2b and c. The ferroelectric nanostructures were spherical rather than islet (or mesa) evidenced by the contact angle over 90°. The contact angles were analyzed through enlarged TEM images in the supporting information (Figure S1). As we recall the experimental procedures, inverse micelles containing TiO$_2$ sol–gel solutions
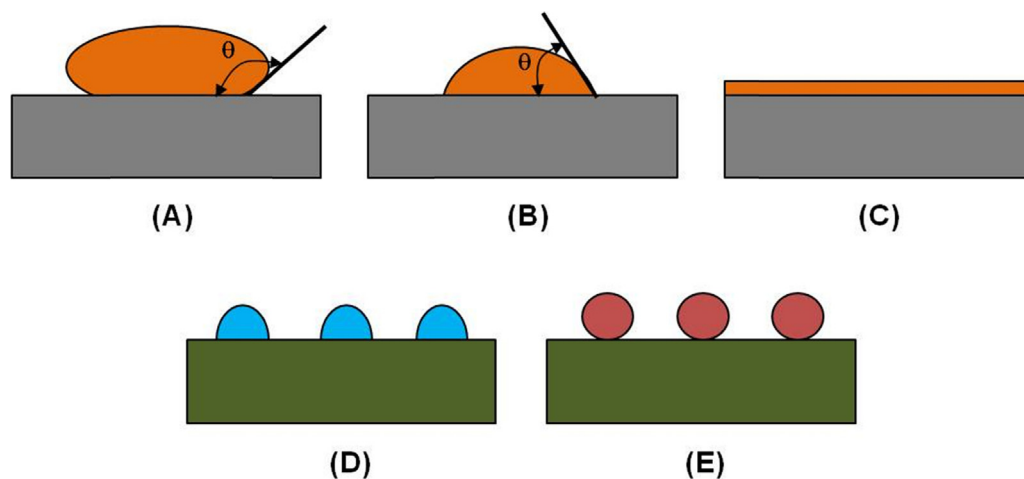
Fig. 1. Schematics of (A) nonwetting ($\theta > 90°$), (B) wetting ($\theta < 90°$), (C) spreading ($\theta = 0°$) of a liquid on a solid, (D) nanoislands ($\theta < 90°$), (E) overhanging nanodots ($\theta > 90°$) on a substrate.
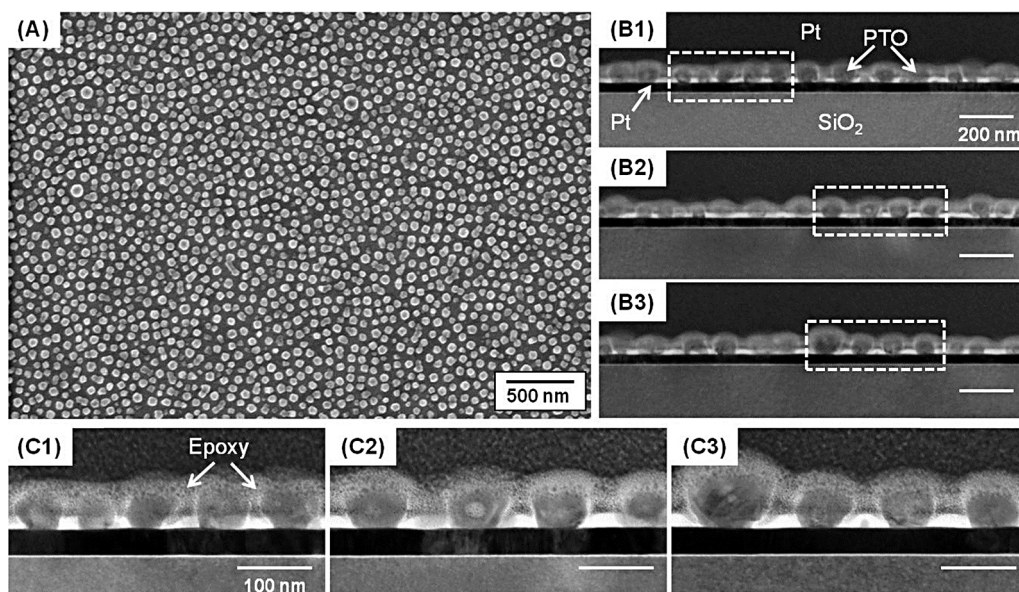
Fig. 2. (A) SEM image of highly cross-packed circular PTO nanodot arrays, (B) cross-sectional TEM images of PTO nanodot arrays on Pt bottom electrode, (C) enlarged TEM image of the area marked by a dashed square in (B).

were hexagonally packed on Pt substrates despite the substrates being rough and polycrystalline. Their average roughness and grain size were 3.557 nm and 300 nm (shown in Figure S2). Then O_2 plasma removed the spherical polymer templates by forming amorphous TiO_2. During the PbO reaction at the elevated temperature, the overhanging TiO_2 nanodots were changed into the polygonal shaped PTO nanodots due to the surface energy anisotropy of the PTO crystal.

Furthermore, we investigated the crystalline orientation of the PTO nanodots. Fig. 3a illustrates a cross-sectional high-resolution TEM (HRTEM) image of the PTO nanodot on the underlying Pt layer; enlarged TEM images of the dashed squares are presented in Fig. 3b–d. Highly oriented (1 0 1), (1 1 0), (1 1 1) and (1 0 0) PTO

planes were observed. The distances between adjacent planes of (1 0 1), (1 1 0), (1 1 1) and (1 0 0) are 2.8, 2.7, 2.4 and 3.8 Å, respectively. These are consistent with the spacing of each plane identified in the literature [23]. Interestingly, the (1 0 1) and (1 1 0) PTO planes were observed on the adjacent Pt layer, whilst the (1 0 0) PTO planes appeared near the free surface of the PTO nanodot and the (1 1 1) planes were located in the center of the PTO nanodot. We thought that the mixed orientations would be related to stoichiometric conditions: the (1 1 1) orientation (center of the PTO nanodot) is related to nucleation with Ti-rich conditions, whist the (1 0 0) orientation (top of the PTO nanodot) is linked with nucleation with Pb-rich conditions [24]. As previously mentioned, the PTO nanodot was created by the reaction between PbO vapor and TiO_2 solid. Unlike
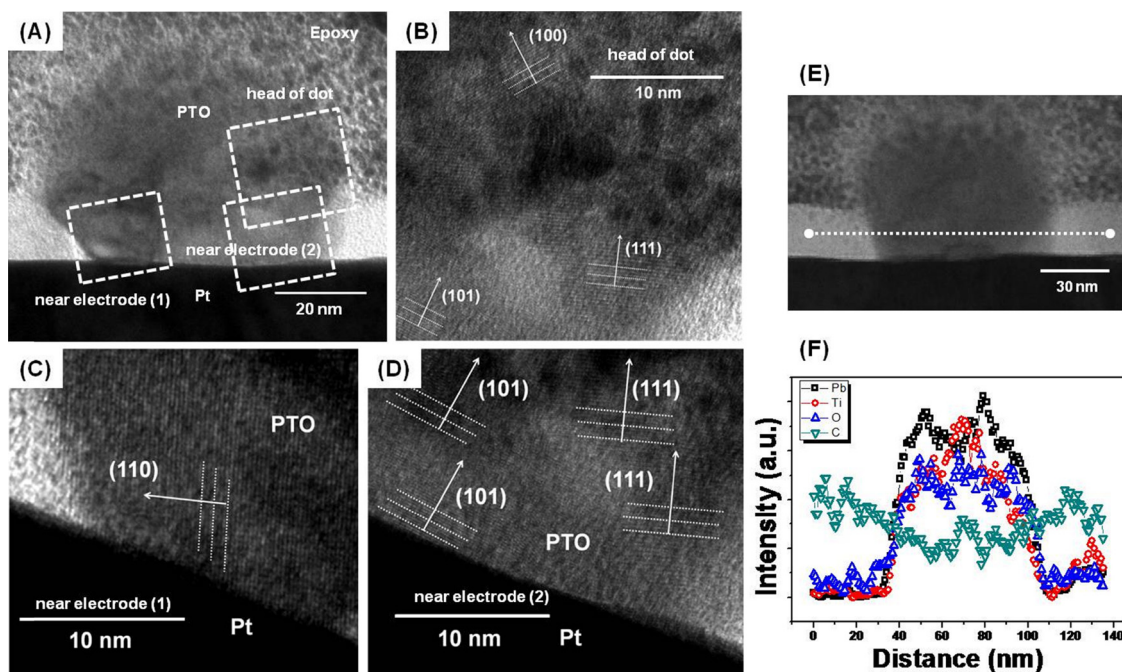
Fig. 3. (A) HRTEM image of sphere shaped PTO nanodot on Pt. An enlarged TEM images of (B) the head of dot, (C) near-electrode (1), (D) near-electrode (2) in (A) were presented. (E) A cross-sectional TEM image of PTO nanodot with a dashed line indicating EDS line-scan and (F) EDS line scan of the PTO nanodot along the dashed line in (E).

chemical vapor deposition or atomic layer deposition, directional atomic bombardment should be considered in the PbO vapor phase sputtering and it can affect PbO re-evaporation. The strong affinity of TiO_2 to PbO also prevents PbO desorption. These would result in different PbO flux surrounding the TiO_2 seeds. The (1 0 1) and (1 1 0) PTO planes, in addition, would be related to the surface enthalpy of TiO_2 surfaces. It is known that the surface enthalpy of its (1 0 0) surface is larger than that of its (1 1 0) surface: calculated values of the (1 0 0) and (1 1 0) surfaces are 3.7 J/m^2 and 2.6 J/m^2. In our study, our amorphous TiO_2 nanodots would start to crystallize at the interface between TiO_2 and Pt and subsequently have (1 1 0) facets to reduce the surface energy during the PbO vapor phase reaction at the elevated temperature. Direct heating to the TiO_2 nanodots allowed for the crystallization of an amorphous TiO_2 phase to a pure anatase TiO_2 phase and the anatase (1 0 1) diffraction peak was detected by high resolution XRD (shown in Fig. 4). Such phase transition could result in the (1 0 1) and (1 1 0) PTO planes. (1 1 0) PTO can be also formed because of the in-plane strain during the phase transition on cooling (from paraelectric to ferroelectric) [25,26]. Fig. 3e shows the cross-sectional TEM image of the PTO nanodot on the [0 1 0] zone axis, where the dashed line indicates the energy dispersive X-ray spectroscopy (EDS) line scan. Simultaneously recorded EDS line scans are presented in Fig. 3f. The EDS features in the TEM results were used to map regions containing Pb, Ti, O and C elements in the PTO nanodot. An electron beam was scanned across the selected region and the resultant X-ray emission spectrum was recorded. The white contrast between the PTO nanodots was confirmed as residual carbon, as shown in Fig. 3f. The EDS analysis also manifests the precise boundaries of the Pb, Ti and O elements in the PTO nanodot as compared to the surrounding area. We could observe Pb-rich (surface) and Ti-rich (heart) areas in the PTO nanodot and this corresponds to the formation of the (1 0 0) and (1 1 1) PTO planes mentioned above. Notably, the spherical PTO nanodot was fixed on the Pt surface by the supporting carbon, which might originate from residual block copolymers.

We henceforth made a further investigation regarding the effect of TiO_2 crystallinity on the crystalline orientation and ferroelectric properties of PTO nanodot arrays. Fig. 4a shows high resolution XRD patterns of TiO_2 nanoseeds before and after a post-annealing treatment at 400 °C for 5 h in a box furnace. Only an anatase (1 0 1) peak made an appearance after the post-annealing treatment. The anatase is not an equilibrium phase of TiO_2, albeit, it would be formed since anatase has lower surface free energy and is less closely packed than rutile [REF]. After PbO vapor reaction both amorphous and anatase TiO_2 nanoseeds were transformed to PTO nanodots. The PTO nanodots originated from amorphous and anatase TiO_2 seeds had mixed orientations of PTO(1 0 0), PTO(1 0 1) and PTO(1 1 1) without any pyrochlore phase (Fig. 4b). Interestingly, the positions of PTO(1 0 0) and PTO(1 1 1) were perfectly matched together, whilst PTO(1 0 1) peaks were slightly deviated each other (Fig. 4c). The observed positions of PTO(1 0 1) crystallized from amorphous and anatase TiO_2 seeds were 31.81° and 31.59°. This indicates that the PTO nanodots prepared from anatase titania were more (1 0 1)-oriented than those prepared from amorphous titania since bulk reference positions of PTO(1 0 1) and PTO(1 1 0) are 31.40° and 32.48°. N.A. Pertsev et al. suggested that the in-plane strain in thin films would lead to PTO(1 1 0) orientation during phase transition from paraelectric phase to ferroelectric phase [25]. Y. Cho et al. confirmed the existence of PTO(1 1 0) as a monoclinic phase band between PTO(1 0 1) planes [26]. SEM and PFM images of PTO nanodots mentioned above can be found in Figure Six. In the SEM observation, PTO nanodots originated from anatase TiO_2 seeds (55.87 ± 4.76 nm) were slightly larger than those originated from amorphous TiO_2 seeds (50.47 ± 3.71 nm). In the PFM observation, excluding a few dots with a single domain structure, most dots were composed of a
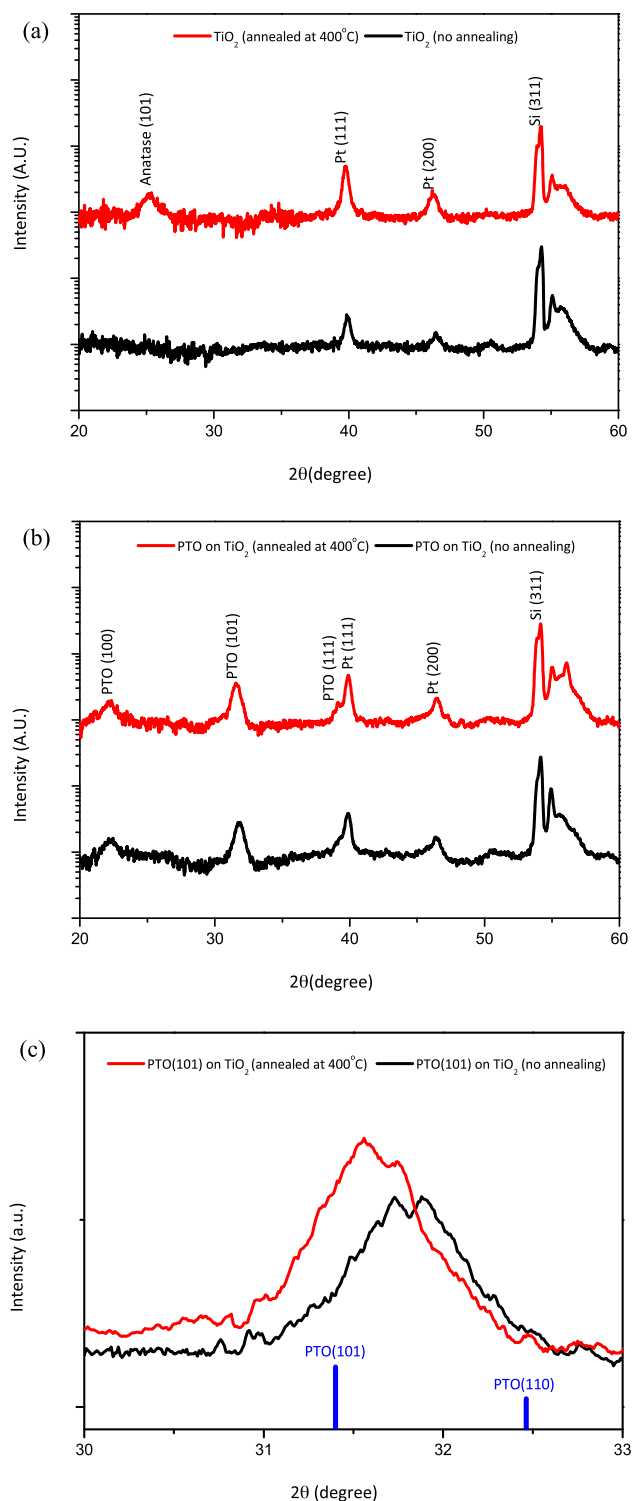

Fig. 4. High resolution XRD patterns of TiO_2 and PTO nanodots before and after annealing at 400 °C.

multi-domain structure with evidence of mixed phase contrasts within one dot.

We also investigated the ferroelectric switching properties of PTO nanodot arrays based on the PFM study. The effective d_{33} piezoresponse hysteresis loops of PTO nanodots grown on differently prepared TiO_2 seeds were obtained at 17 kHz. Typical hysteresis loops measured from PTO nanodots are presented in Fig. 5. The hysteresis loops were saturated within the range of
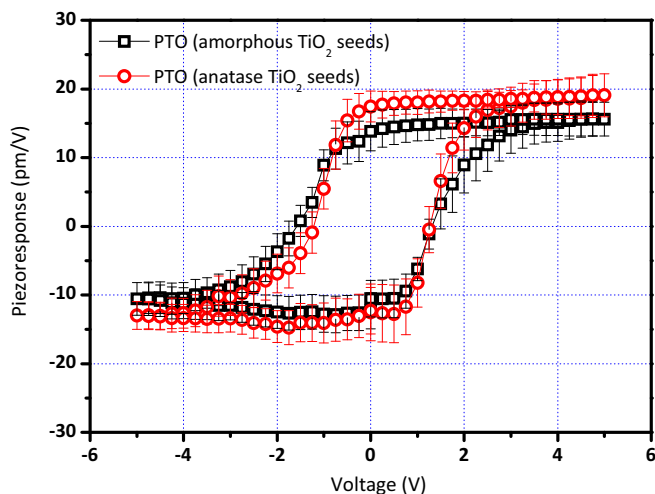
Fig. 5. d_{33} piezoresponse hysteresis loops of overhanging PTO nanodots grown on amorphous and anatase TiO_2 nanodots.

the bias applied and the remnant piezoresponse ($d_{33,r}$) values of PTO nanodots grown on amorphous and anatase TiO_2 seeds were 13.21 pm/V and 14.99 pm/V. The $d_{33,r}$ is equal to $(|d_{33}^+|+|d_{33}^-|)/2$, where d_{33}^+ and d_{33}^-, respectively refer to the upward and downward remnant piezoelectric states. The increase in $d_{33,r}$ would be correlated with the crystallinity of TiO_2 nanoseeds, which allowed for more (1 0 1) orientation of the PTO nanodots. The vertical shift in hysteresis loop referred to d_{33} offset, which is equal to $(d_{33}^+ + d_{33}^-)/2$. The d_{33} offset values of PTO nanodots formed on amorphous and anatase TiO_2 seeds were 0.63 pm/V and 2.465 pm/V, respectively. Previously, we reported that the vertical shifts in PTO thin films, which were fabricated via PbO gas phase reaction with TiO_2 seed layers in a sputtering chamber, were closely related to the residual stress states [27]. We think that the compressive stress in the PTO nanodots restricted the motion of Ti^{4+} ions, when they move downwards at the nanodot/substrate interface, whilst that of Ti^{4+} ions into upward direction was improved by the stretching at the free surface; therefore, the upward polarized domains (positive polarization) exhibit a larger piezoelectric response when compared to downward ones (negative polarization). We speculate that more compressively stressed PTO nanodots would exhibit a larger positive d_{33} offset value. However, the evaluation of the residual stress states at nanoscale is beyond the scope of this study.

4. Conclusion

We presented overhanging PTO nanodot arrays with a reduced contact area achieved by the indirect deposition of ferroelectric materials. We demonstrated that the high surface energy of TiO_2 contributed to the formation of spherical PTO nanodot arrays. HRTEM images and EDS analysis confirmed the origin of mixed orientations within the PTO nanodot. In addition, we found that the

crystallinity of the starting TiO_2 nanoseeds would have an influence on their orientation and ferroelectric switching properties. Currently, we will explore the evolution of residual stress in the PTO nanodots related to the structural change in the starting TiO_2 seeds. This will encourage their use in next-generation memory and high-sensitivity sensory module.

Acknowledgements

Appendix A. Supplementary data

Supplementary material related to this article can be found, in the online version, at http://dx.doi.org/10.1016/j.apsusc. 2014.06.134.

References

[1] O. Aucello, J.F. Scott, R. Ramesh, Phy. Today 51 (1998) 22.
[2] J. Junquera, P. Ghosez, Nature 422 (2003) 506.
[3] P.R Evans, X. Zhu, P. Baxter, M. McMillen, J. McPhillips, F.D. Morrison, J.F. Scott, R.J. Pollard, R.M. Bowman, J.M. Gregg, Nano Lett. 7 (2007) 1134.
[4] X. Chen, S. Xu, N. Yao, Y. Shi, Nano Lett. 10 (2010) 2133.
[5] D.D. Fong, G.B. Stephenson, S.K. Steriffer, J.A. Eastman, O. Aucello, P.H. Fuoss, C. Thompson, Science 304 (2004) 1650.
[6] A. Hoffmann, T. Jungk, E. Soergel, Rev. Sci. Instrum. 78 (2007) 016101.
[7] N. Odagawaa, Y. Cho, Appl. Phys. Lett. 89 (2006) 192906.
[8] I. Vrejoiu, M. Alexe, U. Gösele, J. Vac. Technol. B 27 (2009) 498.
[9] A. Ruediger, T. Schneller, A. Roelofs, S. Tiedke, T. Schmitz, R. Waser, Appl. Phys. A 80 (2005) 1247.
[10] K. Lefki, J.M. Dormans, J. Appl. Phys. 76 (1994) 1764.
[11] M. Alexe, C. Harnagea, W. Erfurth, D. Hesse, U. Gösele, Appl. Phys. A: Mater. Sci. Poc. 70 (2000) 247.
[12] C. Harnagea, M. Alexe, J. Schilling, J. Choi, R.B. Wehrspohn, D. Hesse, U. Gösele, Appl. Phys. Lett. 83 (2003) 1827.
[13] Y. Kim, H. Han, Y. Kim, W. Lee, M. Alexe, S. Baik, J.K. Kim, Nano Lett. 10 (2010) 2141.
[14] J. Kim, J. Hong, M. Park, W. Zhe, D. Kim, Y.J. Jang, D.H. Kim, K. No, Adv. Funct. Mater. 21 (2011) 4277.
[15] M. Park, Y.-Y. Choi, J. Kim, J. Hong, H.W. Song, T.-H. Sung, K. No, Soft Matter 8 (2012) 1064.
[16] P. Muralt, J. Appl. Phys. 100 (2006) 051605.
[17] A.A. Levchenko, G. Li, J. Boerio-Goates, B.F. Woodfield, A. Navrotsky, Chem. Mater. 18 (2006) 6324.
[18] W. Lee, H. Han, A. Lotnyk, M.A. Schubert, S. Senz, M. Alexe, D. Hesse, S. Baik, U. Gösele, Nat. Nanotech. 3 (2008) 402.
[19] B.J. Rodriguez, X.S. Gao, L.F. Liu, W. Lee, I.I. Naumov, A.M. Bratkovsky, D. Hesse, M. Alexe, Nano Lett. 9 (2009) 1127.
[20] J.Y. Son, Y.H. Shin, S. Rye, H. Kim, H.M. Jan, J. Am. Chem. Soc. 131 (2009) 14676.
[21] J.-M. Zhang, Q. Pang, K.-W. Xu, V. Ji, Surf. Interface Anal. 40 (2008) 1382.
[22] E. Heifets, W.A. Goddard III, Phys. Rev. B 69 (2004) 035408.
[23] O. Yamaguchi, A. Narai, T. Komatsu, K. Shimizu, J. Am. Ceram. Soc. 69 (1986) C–C256.
[24] J. Ziolkowski, Surf. Sci. 209 (1989) 536.
[25] N.A. Pertsev, A. Emel'yanov, Yu, Phys. Solid State 39 (1997) 109.
[26] S.K. Choi, S.H. Ahn, W.W. Jung, J.C. Park, S.A. Song, C.B. Lim, Cho Yasuo, Appl. Phys. Lett. 88 (2006) 052901.
[27] J. Kim, S. Hong, S. Bühlmann, Y. Kim, M. Park, Y.K. Kim, K. No, J. Appl. Phys. 107 (2010) 104112.